Forcing of the deep ocean circulation in simulations of the Last Glacial Maximum

A. Schmittner, K. J. Meissner, M. Eby, and A. J. Weaver

School of Earth and Ocean Sciences, University of Victoria, Victoria, British Columbia, Canada

Received 15 February 2001; revised 14 August 2001; accepted 18 September 2001; published 9 May 2002.

[1] From the interpretation of different proxy data it is widely believed that the North Atlantic thermohaline circulation during the maximum of the last ice age ~21,000 years ago was considerably weaker than today. Recent equilibrium simulations with a coupled ocean-atmosphere-sea ice model successfully simulated a reduction in North Atlantic Deep Water (NADW) formation consistent with reconstructions. Here we examine the influence of different air-sea fluxes on simulated changes in the deep ocean circulation between the Last Glacial Maximum and present day. We find that changes in the oceanic surface freshwater fluxes are the dominant forcing mechanism for the reduced Atlantic overturning. Diminished export of freshwater out of the Atlantic drainage basin through the atmosphere decreases surface salinities in the North Atlantic, leading to less NADW formation in the colder climate. Changes in heat fluxes, which lead to increased sea surface densities in the North Atlantic and therefore to an enhanced overturning, are of secondary importance. Wind stress variations seem to play a negligible role. The degree to which the Atlantic freshwater export and hence the NADW formation are reduced depends on the formulation of the atmospheric hydrological cycle and on the strength of the overturning in the present-day simulation. Simulated changes in sea surface properties for a large variety of overturning strengths are compared with different reconstruction data sets. The results depend strongly on the data set used. Sea surface temperature reconstructions from Climate: Long-Range Investigation, Mapping, and Prediction (CLIMAP) and earlier salinity reconstructions based on planktonic foraminifera are most consistent with a significant reduction of the circulation, while recent reconstructions using dinocyst assemblages allow no unequivocal conclusion. *INDEX TERMS:* 4267 Oceanography: General: Paleoceanography; 4255 Oceanography: General: Numerical modeling; 1635 Global Change: Oceans (4203); 1620 Global Change: Climate dynamics (3309); *KEYWORDS:* North Atlantic Deep Water, thermohaline circulation, Last Glacial Maximum, numerical simulations, model evaluation, reconstructions

1. Introduction

[2] Interpretations of different proxy records derived from deep-sea sediment cores suggest that deep water properties during the maximum of the last glacial were substantially different from today. *Boyle* [1995] summarizes the paleoceanographic evidence for changes in the Atlantic deep water masses. He concludes that during the Last Glacial Maximum (LGM) the formation rate of deep water in the North Atlantic was reduced but most likely did not cease completely. The spatial distribution of characteristic properties of North Atlantic Deep Water (NADW) (e.g., low-nutrient and high $\delta^{13}C$ content) during the LGM shows that it was confined to shallower depths than today [*Duplessy et al.*, 1991]. More of the deep Atlantic was instead filled with high-nutrient water of southern origin.

[3] On the other hand, *Yu et al.* [1996] deduce no weaker outflow of NADW into the Southern Ocean based on the analysis of radiochemical data ($^{231}Pa/^{230}Th$ ratios). *Marchal et al.* [2000] showed that errors in measured Atlantic mean $^{231}Pa/^{230}Th$ ratios do not rule out a twofold reduction of the deep water formation but that data from the North Atlantic suggest that the thermohaline circulation (THC) was reduced by no more than 30%. Additional evidence for a reduced Atlantic THC comes from a reconstruction of the Gulf Stream strength [*Lynch-Stieglitz et al.*, 1999] and from neodymium isotope ratios [*Rutberg et al.*, 2000].

[4] While modeling studies of the glacial climate with atmosphere only models [e.g., *Manabe and Broccoli*, 1985] have been performed for a long time, dynamical ocean models have been applied only recently. The first successful attempt to model the deep ocean circulation during the LGM was a study with a simplified ocean model. Relaxing surface values of temperature and salinity to reconstructions (restoring boundary conditions), *Fichefet et al.* [1994] showed that NADW formation was significantly reduced in their zonally averaged model. This result was qualitatively verified with a more complex three-dimensional ocean general circulation model (GCM) [*Seidov et al.*, 1996]. However, it is well known that steady states in an ocean model under restoring boundary conditions are not necessarily stable under more realistic boundary conditions or if coupled to an atmospheric model [*Bryan*, 1986; *Weaver and Sarachik*, 1991; *Tziperman*, 1997].

[5] Three coupled ocean-atmosphere-sea ice models were recently used to investigate the glacial circulation. *Weaver et al.* [1998, 2001] showed a weakening of the Atlantic overturning and a shallower flow of NADW. In the study of *Meissner and Gerdes* [2002] the rate of NADW formation was also decreased, but the flow depth has not changed much. *Ganopolski et al.* [1998] report similar circulation strength but a southward shift of convection sites and a shallower flow of NADW. However, the influences of the different air-sea fluxes on simulated changes of the deep ocean circulation have not been examined so far. This is one objective of the present study, which we address in section 3 following a brief description of the model and experimental design in section 2. Additional sensitivity experiments to the parameterization of the atmospheric hydrological cycle, effects of wind forcing, and the influence of initial conditions are described in section 4. Another purpose of this paper is a comparison of modeled sea surface properties with reconstructions, which we present in section 5. This is undertaken both as a means of evaluating the model simulations as well as to determine the representation of the North Atlantic

0883-8305/02/2001PA000633$12.00

Table 1. Model Experiments[a]

	$\mathbf{F}_q$	$\mathbf{u}_q$	τ
PD	equation (2a)	–	NCEP
LGM	equation (2a)	–	NCEP
LGM PD_FWF	see footnote a and text	see footnote a and text	
PD_ADV_1	equation (2b)	NCEP	NCEP
LGM_ADV_1	equation (2b)	NCEP	NCEP
LGM_ADV_1A	equation (2b)	NCEP + GFDL anomalies	NCEP
LGM_ADV_1B	equation (2b)	NCEP + GFDL anomalies	NCEP + GFDL anomalies
PD_ADV_2	equation (2b)	GFDL PD	NCEP
LGM_ADV_2	equation (2b)	GFDL LGM	NCEP

[a] Equation (2a) is used for the horizontal moisture transport in the model version with purely diffusive atmospheric moisture transport $\mathbf{F}_q$, and (2b) is used if advective transport is included. The moisture advection velocities $\mathbf{u}_q$ and wind stress values τ are either taken from the (present day) monthly climatology of the NCEP reanalysis or from LGM and PD simulations of the Geophysical Fluid Dynamics Laboratory (GFDL) atmospheric GCM. Experiment LGM PD_FWF uses the same parameters as experiment LGM except for the surface freshwater flux, which was fixed to values from the PD integration.

THC most consistent with a particular reconstruction. In section 6 we give an interpretation and a discussion of the results.

2. Model Description and Experimental Setup

[6] We use the University of Victoria (UVic) coupled model, which consists of a two-dimensional latitude-longitude energy-moisture balance model of the atmosphere based on *Fanning and Weaver* [1996] coupled to a three-dimensional ocean primitive equation model (Modular Ocean Model, version 2 [*Pacanowski*, 1995]). The dynamic-thermodynamic sea ice component [*Bitz et al.*, 2001] is based on the models of *Semtner* [1976] and *Hunke and Dukowicz* [1997]. The model version used here is described in some detail by *Weaver et al.* [2001]. It is forced by seasonal variations in solar insolation at the top of the atmosphere and by seasonally varying wind stress at the ocean surface. Boundary conditions for the LGM simulations are similar to those in the work of *Weaver et al.* [1998, 2001], namely, orbital parameters for 21 ka used in the calculation of solar insolation, an atmospheric CO_2 concentration of 200 ppm, and elevated topography using a reconstruction of continental ice sheets [*Peltier*, 1994]. We neglect the influence of the lower sea level on global mean salinity. Wherever continental ice sheets are present, the planetary albedo is raised by 0.18. Two previous equilibrium simulations taken from *Weaver et al.* [2001], one for the present day and one for the LGM, were used to initialize the different experiments. The coupled system was then integrated for 1000 years until a quasi-equilibrium was reached.

[7] We use two different formulations of the atmospheric hydrological cycle that differ in the way moisture is transported horizontally in the model. The vertically integrated balance equation for moisture in the atmosphere can be written as

$$\frac{\partial q}{\partial t} + \nabla \mathbf{F}_q = (E - P)\frac{\rho_o}{\rho_a h_q}, \tag{1}$$

where q is the specific humidity, E and P are evaporation and precipitation, respectively, ∇ is the two-dimensional horizontal divergence operator, and $\mathbf{F}_q$ is the two-dimensional vector of the horizontal moisture flux. The constants ρ_o, ρ_a, and h_q (see *Weaver et al.* [2001] for values) represent water density, surface air density, and atmospheric scale height, respectively. If rainfall occurs over land or snow over land melts, the appropriate amount of fresh water is instantaneously drained into the ocean via one of the river basins. The river catchment areas remain unchanged between present-day and glacial simulations. We use two formulations of the horizontal moisture flux which can be expressed as

$$\mathbf{F}_q = -\kappa(\phi)\nabla q \tag{2a}$$

$$\mathbf{F}_q = -\kappa\nabla q + \beta \mathbf{u}_q q, \tag{2b}$$

where the first term on the right-hand side represents eddy diffusion of specific humidity and the second term represents moisture advection. The latitude-dependent eddy diffusivity is denoted by $\kappa(\phi)$, the constant ratio of vertical mean advective transport to its surface value is given by β, and $\mathbf{u}_q$ is the two-dimensional near-surface wind velocity vector. The two formulations of the hydrological cycle differ mainly in the consideration of advective water vapor transport. In the standard model version (see experiment PD in Table 1) the transport is purely diffusive (equation (2a)). In the advective model version (equation (2b)), $\beta = 0.4$, which is based on previous sensitivity studies, is used, $\kappa = 1 \times 10^6$ m^2/s is a constant, and an additional change is made in the parameterization of the thermal diffusivity (see *Weaver et al.* [2001] for details).

3. Haline Versus Thermal Forcing of the Deep Ocean

[8] The dependence of the ocean-atmosphere heat flux F_T^{OA} on sea surface temperatures (SSTs) is fundamentally different from the dependence of the freshwater (or virtual salinity) flux F_S^{OA} on the sea surface salinity (SSS). While the heat fluxes are directly influenced by local SSTs, the freshwater fluxes do not depend on local SSSs. The latter fact can be seen from (1). Assuming a steady state, the surface freshwater flux $F_S^{OA} = E - P - R$, where R is continental runoff, depends only on the divergence of the atmospheric moisture transport. The decoupling between the SSSs and the freshwater flux makes it possible to examine the effect of thermal and haline forcing separately by fixing the surface freshwater fluxes. Here we follow the methodology of partially coupled simulations [*Mikolajewicz and Voss*, 2000]. Note that this approach differs from mixed boundary conditions, where surface freshwater fluxes are fixed and SSTs are relaxed to prescribed values. In the partially coupled integrations, SSTs can vary freely, and surface heat fluxes interact with the atmosphere as in the fully coupled simulations.

[9] In addition to the fully coupled integrations of the present-day (PD) and Last Glacial Maximum (LGM), a partially coupled integration was performed with LGM boundary conditions but with fixed freshwater fluxes at their present-day values (LGM PD_FWF). Therefore we diagnosed the seasonal cycle of the freshwater fluxes at the ocean surface from the last year of the present-day integration. This diagnosed seasonal cycle was then used in the partially coupled integration LGM PD_FWF as the prescribed surface freshwater fluxes. The difference between the LGM PD_FWF and PD integrations thus isolates the thermal effect

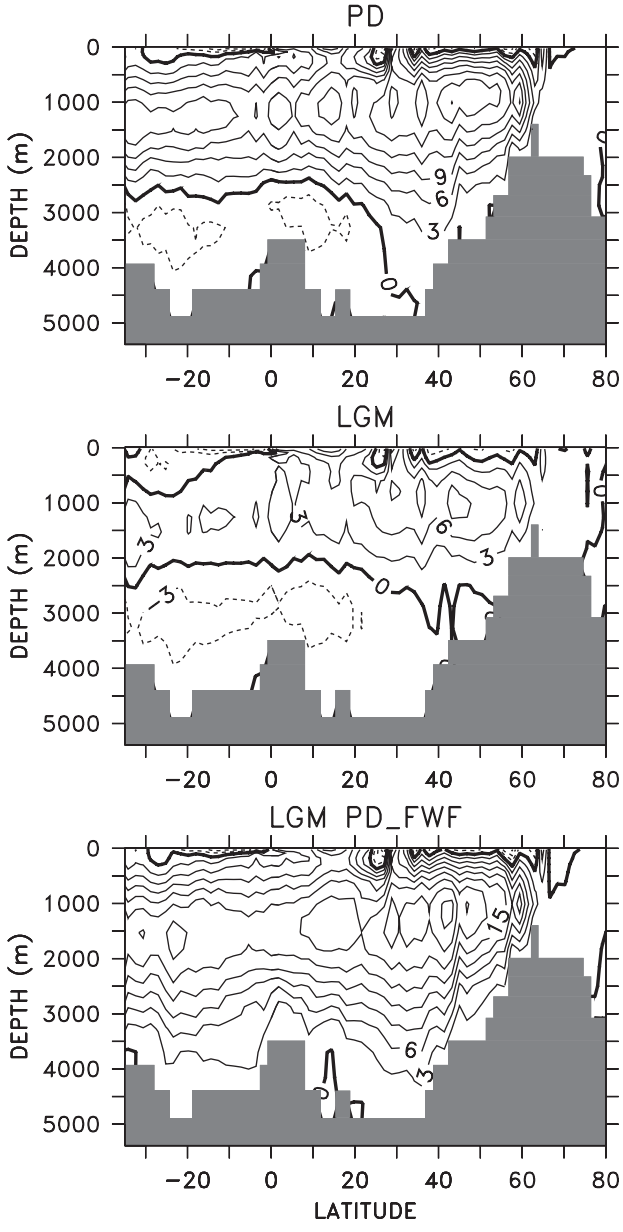

Figure 1. Annual mean meridional overturning stream function in the Atlantic in Sverdrups (1 Sv = 10^6 m^3/s) for (top) the standard present day (middle) and LGM simulations and (bottom) a simulation with LGM boundary conditions but present-day surface freshwater fluxes (see also Table 1). Isoline difference is 3 Sv with negative values given as dashed lines.

on the circulation changes, while the difference between LGM and LGM PD_FWF reveals the effect of changed freshwater fluxes. Note that the momentum fluxes, i.e., wind stress, are kept fixed in all three simulations (PD, LGM, and LGM PD_FWF) at present-day values. We will address the issue of changes in wind stress in section 4.2.

[10] Figure 1 shows the overturning stream function in the Atlantic for the three simulations. In the present-day case the production rate of NADW is ~21 Sv, more than half of which crosses the equator and enters the Antarctic Circumpolar Current (ACC) (see also Table 2). Antarctic Bottom Water (AABW) fills the abyssal Atlantic below ~2500 m and reaches as far north as 30°N. In the simulation of the LGM, deep water formation in the North Atlantic is much weaker (≃11 Sv) and shallower than in the present-day simulation. The circulation of NADW is much more confined to the Northern Hemisphere. AABW advances farther north and fills the deep basin below 2000 m. These values are similar to previous studies with an ocean only model in which SSTs and SSSs were relaxed to reconstructions and modern observations [*Seidov and Haupt*, 1999; *Seidov and Maslin*, 1999].

[11] In the simulation with LGM boundary conditions but fixed present-day surface freshwater fluxes (LGM PD_FWF) the overturning in the Atlantic has slightly increased to 24 Sv. NADW now fills the entire Atlantic, and AABW is noticeably absent. This shows that the thermal forcing alone leads to an increase in NADW formation. Hence the reduction of NADW formation in the fully coupled simulation (LGM) is dominated by changes in the freshwater forcing. Moreover, this result suggests that thermal and haline forcing act in opposite directions, with thermal forcing alone tending to increase NADW formation, and haline forcing acting to reduce it.

[12] The relative abundance of NADW and AABW in the Atlantic depends on their densities [*Stocker et al.*, 1992]. If the density of one of the two water masses increases, this water mass will occupy more volume of the basin. Therefore, in order to better understand the different forcing mechanisms involved in changing the deep Atlantic water masses, we examine the zonally averaged density changes.

[13] In Figure 2 the density differences $\Delta\rho = \rho_{\mathrm{LGM}} - \rho_{PD} \simeq \Delta\rho_T + \Delta\rho_S$ between the LGM and PD experiments and between the LGM PD_FWF and PD experiments are shown, together with the individual contributions of salinity $\Delta\rho_S = \rho(T_{PD}, S_{\mathrm{LGM}}) - \rho(T_{PD}, S_{PD})$ and potential temperature $\Delta\rho_T = \rho(T_{\mathrm{LGM}}, S_{PD}) - \rho(T_{PD}, S_{PD})$. The separation of the total density changes into the individual contributions of temperature, and salinity assumes a linear equation of state. For the relatively small density changes discussed here this assumption is justified.

[14] Since we do not consider the change of global mean salinity due to sea level lowering, density changes between the glacial and present-day simulations are dynamically important. In the fully coupled simulation (LGM) the density of the deep waters in the Atlantic has not changed much compared to the present-day run. However, we see that this is due to the opposing effects of temperature and salinity. While cooling of NADW tends to increase deep densities, freshening leads to lighter deep water. Both effects nearly compensate, resulting in only small overall changes. If surface freshwater fluxes are fixed at present-day values (LGM PD_FWF), the salinity contribution to the changes in deep densities is negligible, leading to a dominance of the thermal effect. NADW gets colder and denser. This does not occur as much for AABW, which is already formed near freezing

Table 2. Model Diagnostics[a]

Experiment	$\Psi_{\max}$	$\Psi_{\max}(35°\mathrm{S})$	$\int_{\mathrm{Atl}} E - P$
PD	21	14	0.26
LGM	11	6	0.16
LGM PD_FWF	25	16	0.26
PD_ADV_1	21	15	0.27
LGM_ADV_1	4	3	0.23
LGM_ADV_1A	14	9	0.26
LGM_ADV_1B	11	9	0.25
PD_ADV_2	26	19	0.41
LGM_ADV_2	22	16	0.38

[a] The maximum overturning stream function in the Atlantic north of 35° S and below 300 m depth is denoted by $\Psi_{\max}$. The outflow of NADW into the Southern Ocean $\Psi_{\max}$ (35°S) is calculated as the maximum overturning stream function at 35° S. The total surface freshwater balance of the Atlantic north of 35° S is denoted by $\int_{\mathrm{Atl}} E - P$. All units are in Sv.

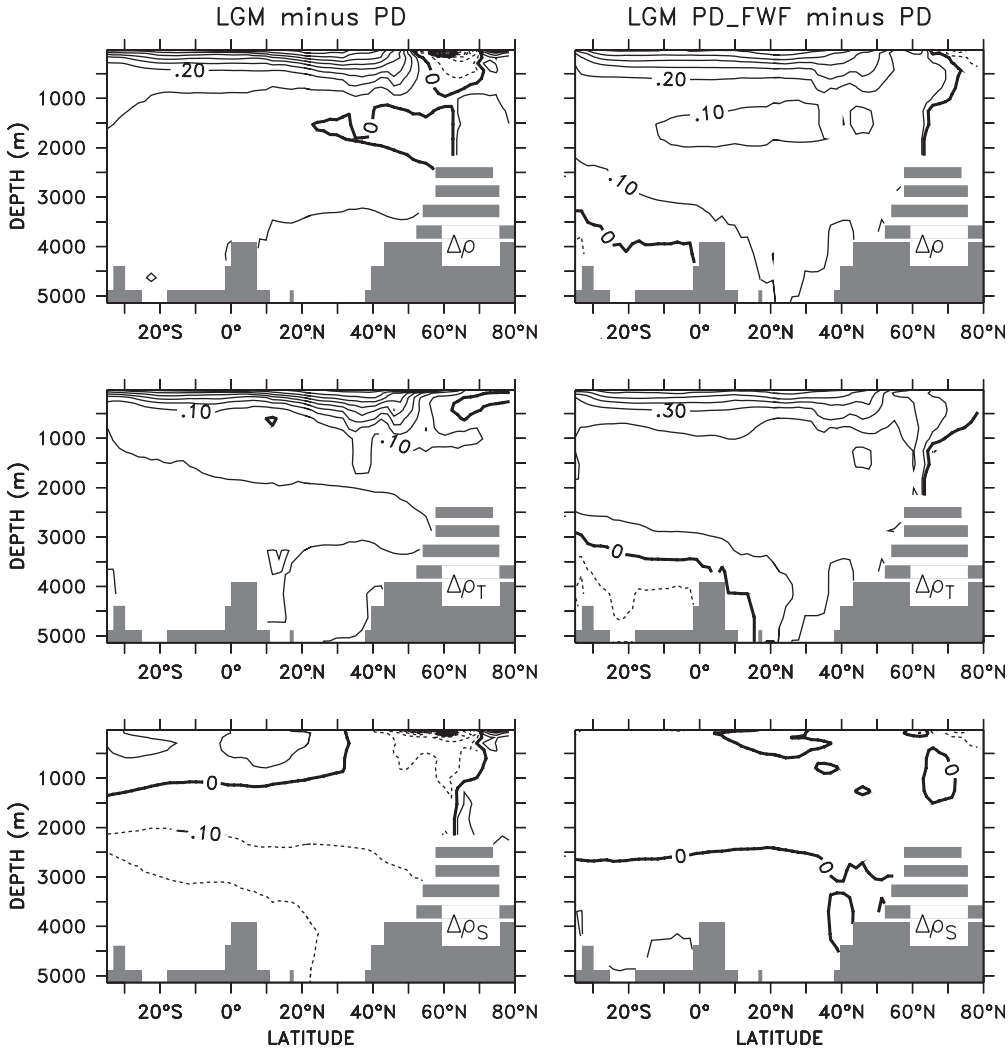

Figure 2. Density differences between (top) runs LGM and PD (left) and LGM PD_FWF and PD (right) decomposed into contributions (middle) from temperature changes $\Delta\rho_T$ and (bottom) from salinity changes $\Delta\rho_S$. Isoline differences are 0.1 kg/m^3 with negative values given as dashed lines.

temperatures in the present-day climate. Hence it cannot be cooled much further, and its density remains approximately constant. Thus, if NADW gets heavier, like in LGM PD_FWF, it acts to force AABW out of the Atlantic basin in accordance with *Stocker et al.* [1992].

[15] In order to better understand the changes in the strength of the Atlantic overturning in the different experiments we examine the zonally averaged depth-integrated steric height, which is defined as

$$\phi = \int_{z=h_0}^{0} \int_{z'=-h_0}^{z} \left(\frac{\overline{\rho(z')}}{\rho_0} - 1 \right) dz' dz, \qquad (3)$$

where ρ_0 = 1035 kg/m^3 is a reference density, $\overline{\rho(z')}$ is the depth-dependent zonally averaged in situ density, and h_0 = 925 m is the approximate depth of no zonally averaged meridional motion. Here ϕ is a measure of the vertically integrated hydrostatic pressure. In a frictional boundary layer it is reasonable to assume that the flow is down pressure gradient. Indeed, earlier studies have shown that the strength of the overturning is roughly proportional to the zonally averaged depth-integrated steric height difference between the southern tip of Africa (around 35°S), where the zonal boundary ends, and the regions of deep water formation around 60°N [*Hughes and Weaver*, 1994; *Wiebe and Weaver*, 1999].

[16] In Figure 3 the difference in zonally averaged depth-integrated steric height between the LGM and LGM PD_FWF simulations and the PD simulation are shown together with the contributions due to temperature and salinity changes. The zonally averaged depth-integrated steric height difference between 35°S and 60°N has clearly decreased between the LGM and PD integrations, consistent with the weaker overturning (see Figure 1). Although the temperature effect is stronger at most latitudes, the effect of salinity changes contributes significantly to the decreased steric height gradient.

[17] In the integration with fixed present-day freshwater fluxes (LGM PD_FWF), salinity changes are no longer important. Note that this does not follow a priori from the fact that the surface freshwater fluxes are fixed since thermally induced circulation changes could alter the salinity distribution. The total change in the gradient of ϕ between 35°S and 60°N between LGM PD_FWF and PD is small, consistent with the similar rate of NADW production. Thus thermal forcing alone is not sufficient for a reduction of the meridional gradient of depth integrated steric height and an

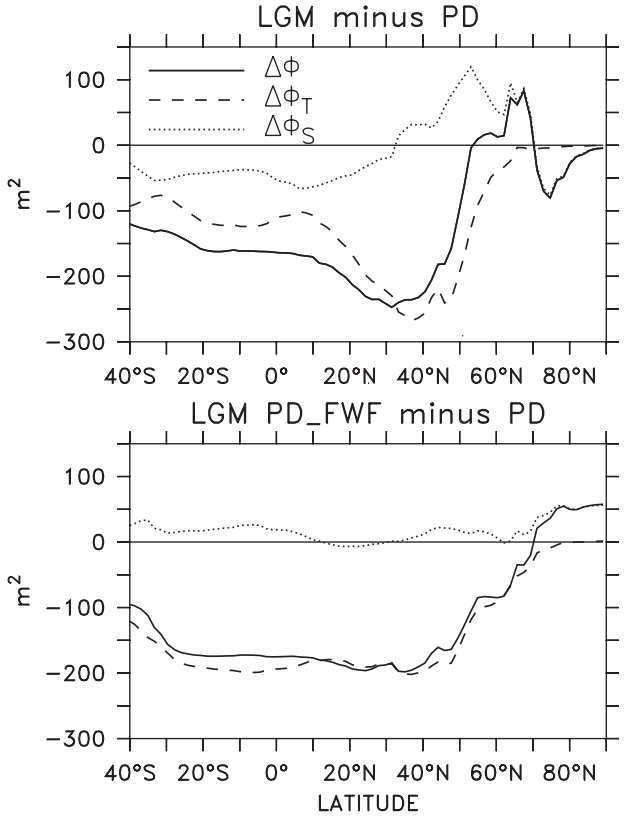

Figure 3. Zonally averaged depth-integrated steric height difference between (top) LGM and PD and (bottom) LGM PD_FWF and PD in the Atlantic. The total difference $\Delta\phi$ is decomposed into contributions from temperature changes $\Delta\phi_T$ and from salinity changes $\Delta\phi_S$.

associated reduction in North Atlantic overturning. Note that although the overturning has increased slightly in experiment LGM PD_FWF, the gradient of ϕ between 35°S and 60°N has decreased slightly. This discrepancy could be caused by violations in the assumptions calculating ϕ, e.g., changing depth of the level of no motion, or it could suggest that the relation between these two quantities is not strictly linear.

4. Sensitivity Experiments

4.1. Sensitivity to Parameterization of Atmospheric Moisture Transport

[18] In section 3 the horizontal transport of water vapor in the atmosphere was parameterized as a purely diffusive process (equation (2a)). Here we include near-surface advection of specific humidity (equation (2b)) as described in section 2. This scheme substantially improves the distribution of precipitation in simulations of the present-day climate [*Weaver et al.*, 2001].

[19] Figure 4 shows the stream function of the zonally integrated flow in the Atlantic for a present-day simulation and a LGM simulation using near-surface moisture advection. In both simulations, wind velocities $\mathbf{u}_q$ for the moisture advection were taken from the present-day climatology of the National Centers for Environmental Prediction (NCEP) reanalysis [*Kalnay et al.*, 1996]. Meridional overturning in the Atlantic in the present-day simulation (PD_ADV_1) is very similar to the simulation with purely diffusive transport (PD in Figure 1). However, in the simulation of the LGM (LGM_ADV_1), deep water formation in the North Atlantic ceases completely. This is in contrast to the run using diffusive water vapor transport (LGM in Figure 1).

[20] Note that keeping the wind velocities $\mathbf{u}_q$ at present-day values for the LGM experiment are not realistic. In order to examine the model sensitivity to changes in wind velocities we add anomalies given by a dynamic atmosphere model. Two equilibrium simulations from an atmosphere model coupled to a mixed layer ocean are used [*Broccoli*, 2000]. Near-surface wind velocities from the present-day simulation are subtracted from those of the LGM simulation in order to obtain the response of the surface winds to the changed boundary conditions. These anomalies are then added to the present-day wind velocities obtained from NCEP. In this section we only apply these wind velocity anomalies to (2b) to compute moisture advection. This approach isolates the effect of surface wind changes on the surface buoyancy forcing of the ocean. In section 4.2 we also analyze the effects of changed near-surface winds on the ocean's surface momentum forcing.

[21] Figure 5 shows the Atlantic meridional overturning in the steady state obtained including near-surface wind velocity anomalies from the Geophysical Fluid Dynamics Laboratory (GFDL) model (experiment LGM_ADV_1A). The maximum overturning is ~14 Sv with ~6 Sv crossing the equator and entering the ACC. The circulation pattern is remarkably different from the one neglecting dynamical changes in the moisture advection (LGM_ADV_1 in Figure 4). The wind velocity anomalies are small compared to the mean wind (not shown). However, even such small changes have a considerable influence on the freshwater balance and can therefore determine the circulation regime of the Atlantic.

4.2. Sensitivity to Changes in Wind Stress

[22] Here we examine the influence of changed low-level winds on the momentum balance at the sea surface. To facilitate this,

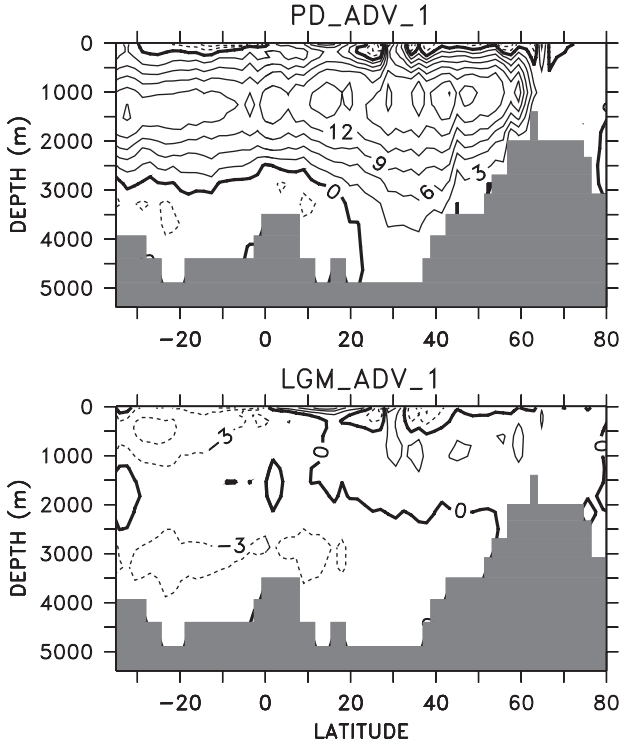

Figure 4. Annual mean meridional overturning stream function in the Atlantic for simulations (top) PD_ADV_1 and (bottom) LGM_ADV_1. Moisture advection velocities $\mathbf{u}_q$ (see (2b)) are used from the present-day climatology of the NCEP reanalysis in both simulations.

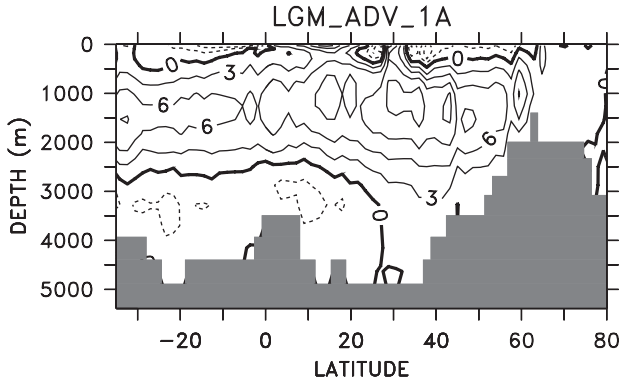

Figure 5. Annual mean meridional overturning stream function in the Atlantic for simulation LGM_ADV_1A. Anomalies from the GFDL model are added to the present-day moisture advection velocities.

experiment LGM_ADV_1A was repeated but now also including wind stress anomalies from the GFDL model. The wind stress anomalies were computed in the same way as the anomalies of near-surface wind velocities used in section 4.1. Comparing the meridional overturning in Figure 6 (experiment LGM_ADV_1B) with the results from experiment LGM_ADV_1A (Figure 5), we see that the changes in wind stress have only a very small influence on the deep circulation.

4.3. Sensitivity to Initial Overturning Strength

[23] Results from two additional experiments, illustrating the dependence of simulated changes in the deep ocean circulation on the strength of the THC in the present-day simulation, will be presented next. In sections 4.1 and 4.2 we have seen that small changes in atmospheric low-level wind velocities can have a substantial impact on the deep circulation of the Atlantic owing to changes in the Atlantic freshwater budget. Using a different data set for present-day low-level winds is therefore likely to result in a different overturning circulation in the Atlantic for the simulation of the modern climate. This is indeed the case as can be seen from experiment PD_ADV_2 in Figure 7. Here wind velocities $\mathbf{u}_q$ from the present-day simulation of the GFDL model were used instead of NCEP reanalysis data (which were used in experiment PD_ADV_1). In experiment PD_ADV_2 the overturning has a maximum of 26 Sv compared to 21 Sv in experiment PD_ADV_1 (see Figure 4).

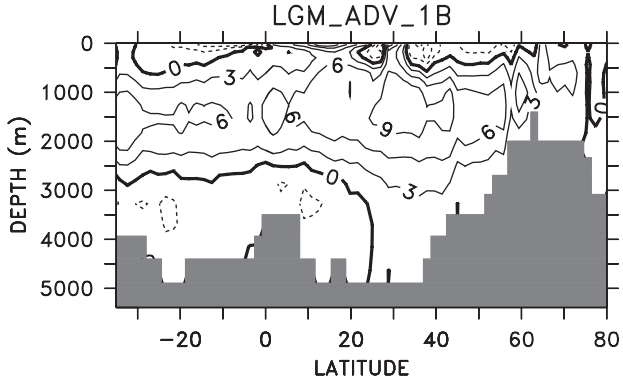

Figure 6. Annual mean meridional overturning stream function in the Atlantic for simulation LGM_ADV_1B. Anomalies from the GFDL model are added to the present-day near-surface wind velocities and to the wind stress at the sea surface.

[24] In the corresponding simulation of the Last Glacial Maximum (LGM_ADV_2), wind velocities $\mathbf{u}_q$ were taken from the LGM simulation of the coupled GFDL model. Thus the anomalies of $\mathbf{u}_q$ between experiments LGM_ADV_2 and PD_ADV_2 are the same as those between experiments LGM_ADV_1A and PD_ADV_1. The comparison of the circulation changes between these two pairs of simulations therefore gives an indication of the influence of the initial (or present day) strength of the THC on the model results.

[25] The reduction of deep water formation between LGM_ADV_2 and PD_ADV_2 is only 3.8 Sv compared with 6.2 Sv between LGM_ADV_1A and PD_ADV_1. This shows that a weaker initial overturning is affected more by a perturbation than a stronger initial overturning, consistent with earlier studies [e.g., *Rahmstorf*, 1996; *Weaver et al.*, 1998].

5. Evaluation of Modeled Sea Surface Properties With Reconstructions

[26] In this section we will use the different simulations of the LGM presented in sections 3 and 4 for a comparison with reconstructions. Although it is widely accepted that the Atlantic THC was significantly reduced during the LGM, the degree to which it was reduced is still under debate [*Boyle*, 1995]. The strengths of the THC in the LGM simulations presented in the previous sections range from a slight increase in overturning for

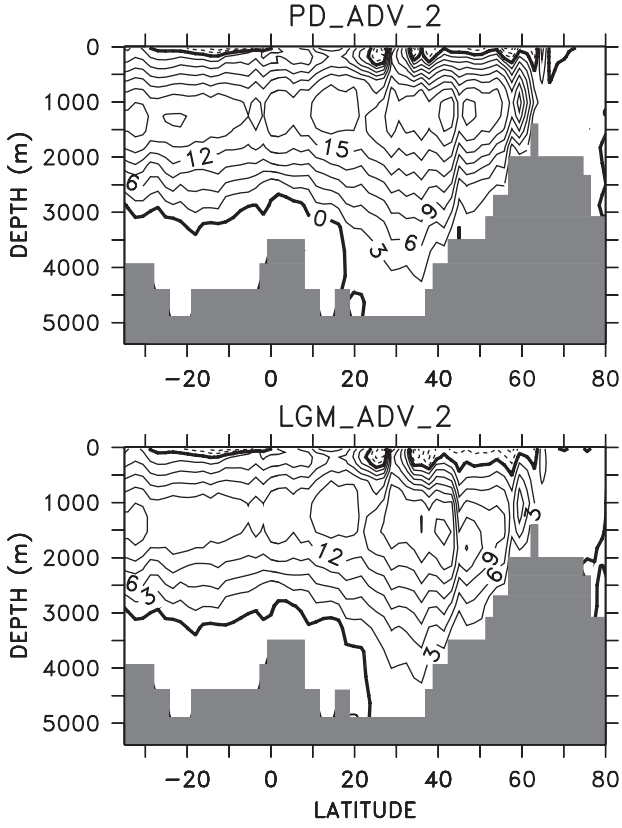

Figure 7. Annual mean meridional overturning stream function in the Atlantic for simulations (top) PD_ADV_2 and (bottom) LGM_ADV_2. Near-surface wind velocities $\mathbf{u}_q$ are used from the present-day (for PD_ADV_2) and from the LGM (for LGM_ADV_2) simulation of the GFDL model.

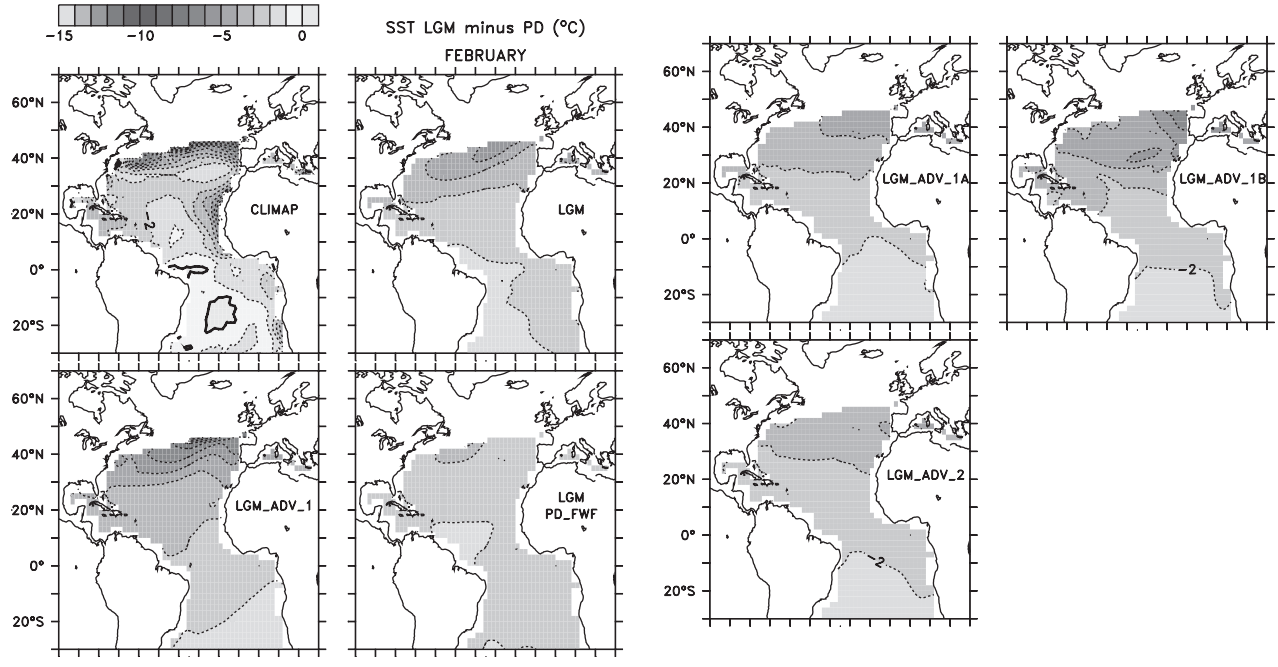

Figure 8. Difference of February sea surface temperatures between the LGM and present day. Top left plot shows CLIMAP reconstruction interpolated to the model grid. Other plots show simulations (experiment name noted over North Africa). Note that only grid points without sea ice in the CLIMAP reconstruction are shown. The model results were masked appropriately. See color version of this figure at back of this issue.

experiment LGM PD_FWF to a total collapse of deep water formation in experiment LGM_ADV_1. It is well known that the strength of the meridional overturning has a strong effect on the distribution of sea surface properties [*Manabe and Stouffer*, 1988]. Therefore our objective is to compare modeled sea surface properties with reconstructions to allow one to assess the likelihood of the possible circulation patterns during the LGM.

5.1. Reconstruction Data Sets

[27] For SST we use reconstructions from Climate: Long-Range Investigation, Mapping, and Prediction (CLIMAP) [*CLIMAP Project*, 1976, 1981] for winter (February) and summer (August). For summer SSS a compilation of reconstructions from *Seidov et al.* [1996] is used in which data from *Duplessy et al.* [1991] and *Sarnthein et al.* [1995] and present-day observations were used to construct a gridded data set for the North Atlantic. The advantage of these data sets is their large spatial coverage. CLIMAP data are global in extent, although here we only use data the Atlantic north of 35°S. The *Seidov et al.* [1996] data set covers the North Atlantic between 10° and 80°N. CLIMAP temperature reconstructions have been subject to a considerable debate in the recent past [e.g., *Mix et al.*, 1999, 2001; *Weaver et al.*, 1998; *de Vernal et al.*, 2000, and references herein]. In section 5.4 we will therefore repeat the analysis with a more recent data set [*de Vernal et al.*, 2000] which, however, covers only the northern North Atlantic between 45° and 65°N.

[28] In order to minimize the effect of systematic model errors in the simulation of the present-day climate on the results of the analysis, we only consider the difference between the LGM and present day. For the CLIMAP SST reconstructions the computation of the anomalies was straight forward since CLIMAP provides present-day SST fields constructed in the same way as the LGM reconstruction. For salinity we subtracted present-day observations from August [*Levitus et al.*, 1994] from the LGM reconstruction.

5.2. CLIMAP SSTs

[29] Figure 8 shows the changes in winter SSTs in the Atlantic between the LGM and present day for the different model

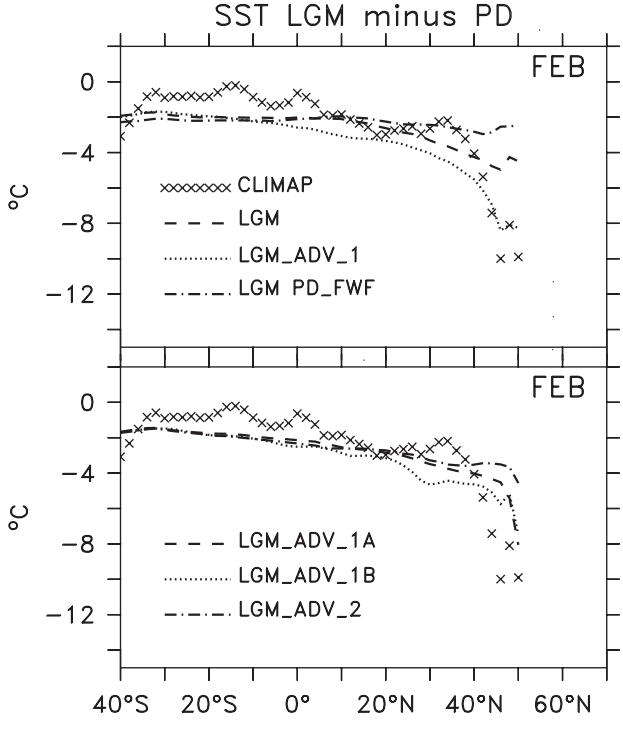

Figure 9. Difference of zonally averaged February sea surface temperatures between LGM and present day.

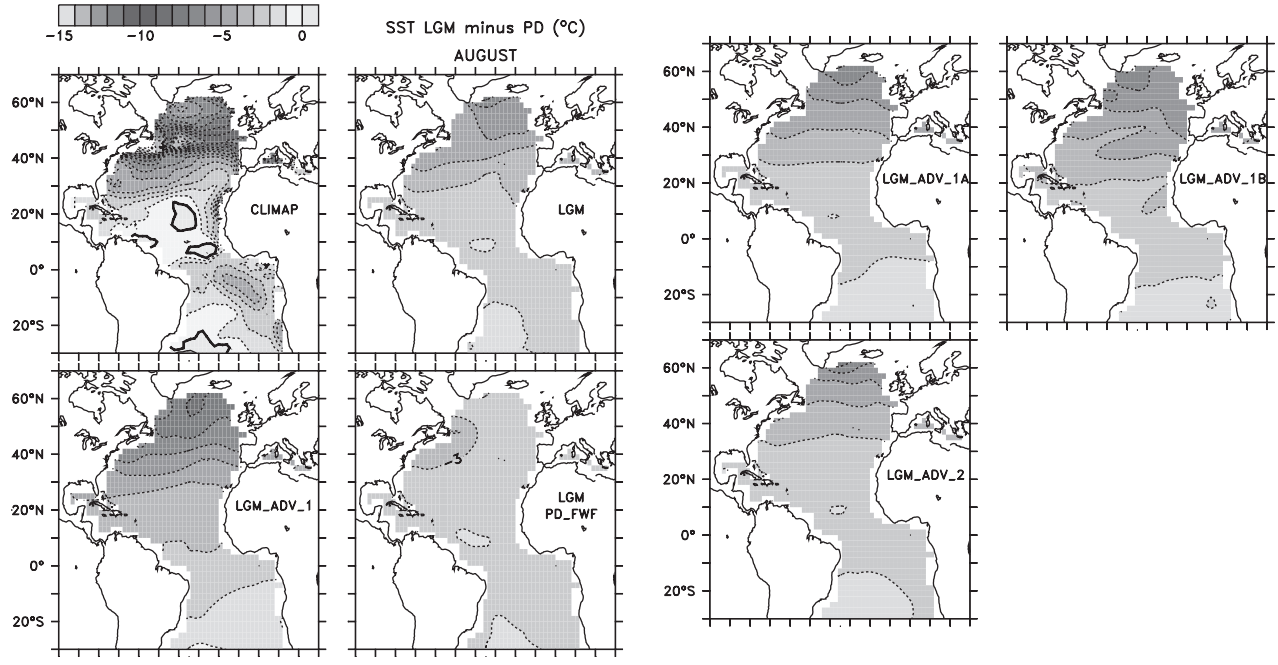

Figure 10. Difference of August sea surface temperatures between the LGM and present day. Top left plot shows CLIMAP reconstruction. Other plots show simulations (experiment name noted over North Africa). See color version of this figure at back of this issue.

simulations together with the reconstruction. Cooling, up to 10°C, in SSTs is strongest near the winter sea ice margin [*Manabe and Broccoli*, 1985]. These large amplitudes are not captured by any of the model simulations. However, in most experiments a pronounced latitudinal gradient with strongest cooling in the north is simulated. A notable exception is experiment LGM PD_FWF, which is the only simulation where the overturning and therefore the northward heat transport by the ocean was not reduced. The simulation with a completely collapsed THC (LGM_ADV_1) shows the strongest cooling in the North Atlantic, most consistent with the reconstructions. However, SSTs in the rest of the basin are considerably colder in experiment LGM_ADV_1 than the CLIMAP data.

[30] The zonally averaged winter SST changes between LGM and PD shown in Figure 9 also seem to suggest that the strong cooling around 50°N in CLIMAP is best simulated by experiment LGM_ADV_1. In Figure 10 summer SST changes are plotted. The CLIMAP summer reconstruction also shows maximum cooling (>12°C) between 40° and 50° N. None of the model experiments captures either the large magnitudes or the correct location of the maximum SST changes. However, as for the case of winter SSTs, a pronounced north-south gradient in the SST changes is present in all simulations except experiment LGM PD_FWF (Figure 11). Note that the north-south gradient in the simulated SST changes depends monotonically on the changes in overturning. The stronger the reduction of the Atlantic THC, the larger the meridional SST gradient. Generally, the variations in the CLIMAP north-south SST gradient seem to be consistent with a reduced THC. The largest disagreement between model results and reconstruction is the strong minimum around 45°N in the CLIMAP data, which is not captured in any of the simulations.

[31] There are three possible reasons for this discrepancy. The first may be related to the fact that the heat transport in the atmospheric energy balance model is entirely diffusive. This parameterization tends to smooth strong SST anomalies through ocean-atmosphere heat flux and subsequent diffusion of temperature anomalies in the atmosphere. Furthermore, the lack of advective heat transport in the atmosphere prevents a correct simulation of the very cold westerly air masses downstream the Laurentide ice sheet. The second reason is related to uncertainties in the CLIMAP data. While in a simulation of an atmospheric GCM coupled to a mixed layer ocean [*Manabe and Broccoli*, 1985] a pronounced minimum of SST changes is simulated at

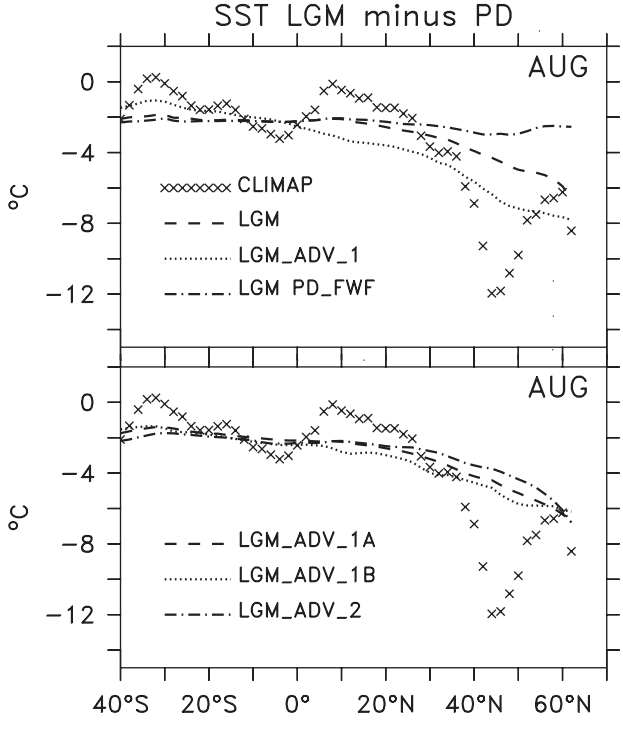

Figure 11. Difference of zonally averaged August sea surface temperatures between LGM and present day.

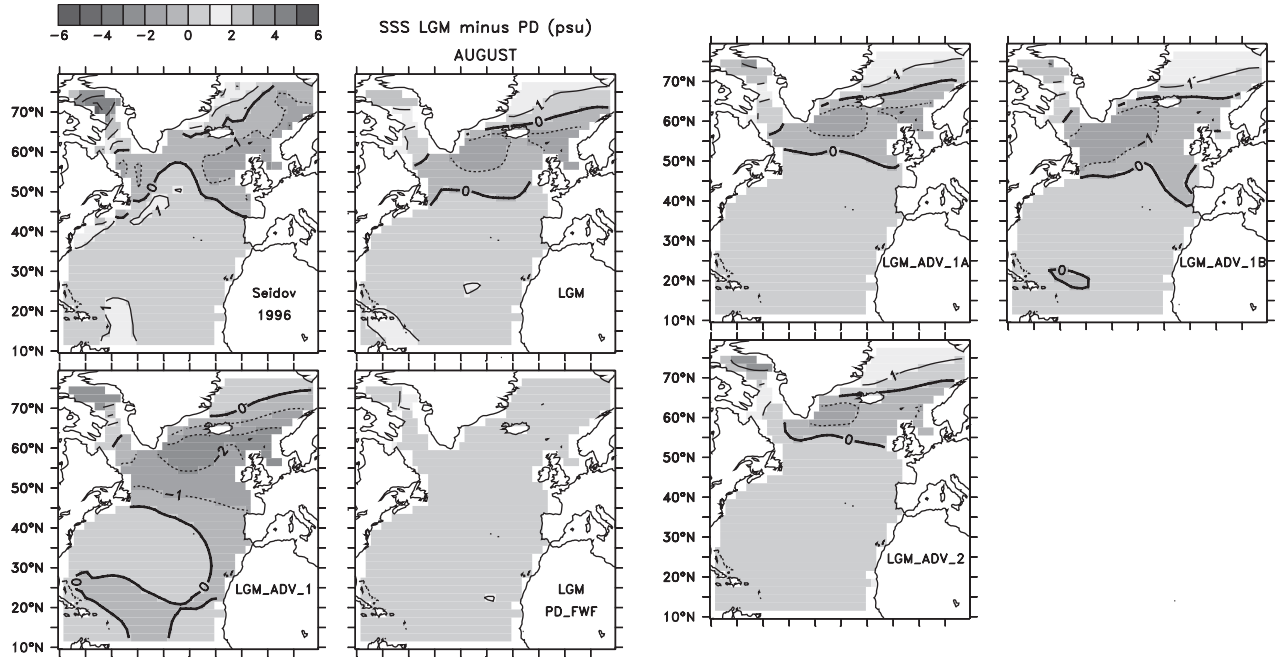

Figure 12. Difference of August sea surface salinities between the LGM and present day. Top left plot shows reconstruction from *Seidov et al.* [1996]; Other panels: simulations (experiment name noted over North Africa). See color version of this figure at back of this issue.

midlatitudes, the large amplitude of this minimum in the CLIMAP reconstruction is not reproduced. Evidence that the CLIMAP reconstruction might be too cold in the northern North Atlantic is also discussed by *de Vernal et al.* [2000]. The third reason is related to a systematical cold bias in our simulations of the present day in the North Atlantic (see also section 6). As pointed out by *Manabe and Broccoli* [1985], the latitude of maximum SST cooling is located near the winter sea ice edge. Since the sea ice edge in our present-day simulation is already too far south, this might contribute to the underestimated cooling in our experiments of the LGM.

[32] In the tropics, all simulations yield cooler SSTs by ~2.2°C irrespective of the season. As already pointed out by *Weaver et al.* [1998], this is slightly colder than CLIMAP estimates but in good agreement with alkenone reconstructions. Here we see that this conclusion is independent of the reduction in Atlantic overturning. However, for the case where the circulation collapses completely (LGM_ADV_1), an interhemispheric gradient in SST reduction is simulated, such that Northern Hemisphere low latitudes experience a slightly stronger cooling and Southern Hemisphere tropics are slightly warmer than in the other experiments. No experiment simulates the pronounced maximum cooling of up to 5°C in the eastern tropical Atlantic as suggested by a recent reconstruction based on foraminiferal estimates [*Mix et al.*, 1999].

5.3. Seidov's SSS

[33] Maps of changes in summer SSSs are shown in Figure 12. Note that 0.8 psu has been artificially added to the salinity fields of the LGM simulations since the global change of the ocean volume due to the build up of the ice sheets has not been taken into account in the simulations. The value of 0.8 psu has been chosen in order to be consistent with the assumptions of *Seidov et al.* [1996] and corresponds to a change in ice volume of $\sim 3.4 \times 10^{16}$ m^3 or a sea level drop of ~86 m, which is on the lower side of present estimates [*Clark et al.*, 2001]. The reconstruction shows freshening of surface waters in the northeastern part of the basin. South of ~50°N, salinity was higher during the LGM according to the reconstruction. All model simulations, except LGM PD_FWF, show a meridional gradient in SSS changes, which is qualitative similar to the reconstructions. Again, similar to the SST changes discussed above, the meridional gradient of the salinity changes is monotonically dependent on the changes of the THC. The stronger the reduction of the overturning, the weaker the northward advec-

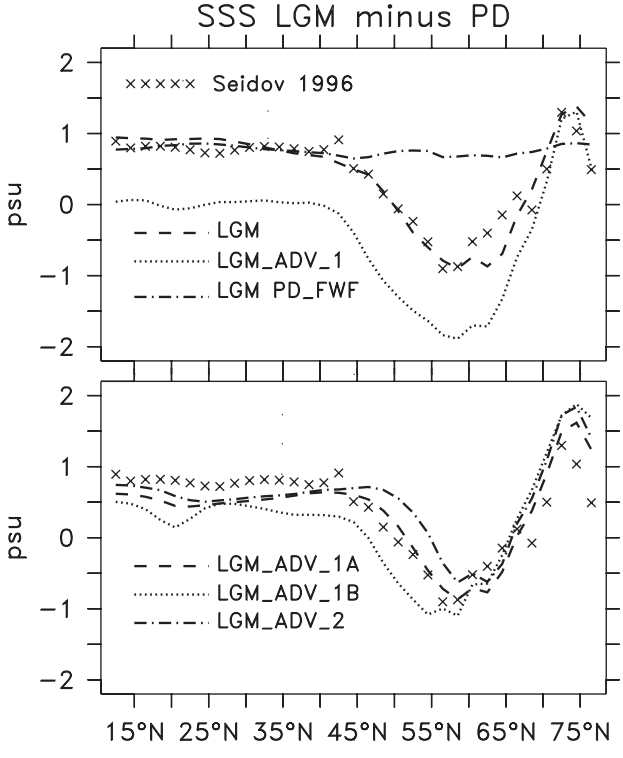

Figure 13. Difference of zonally-averaged August sea surface salinities between LGM and present day.

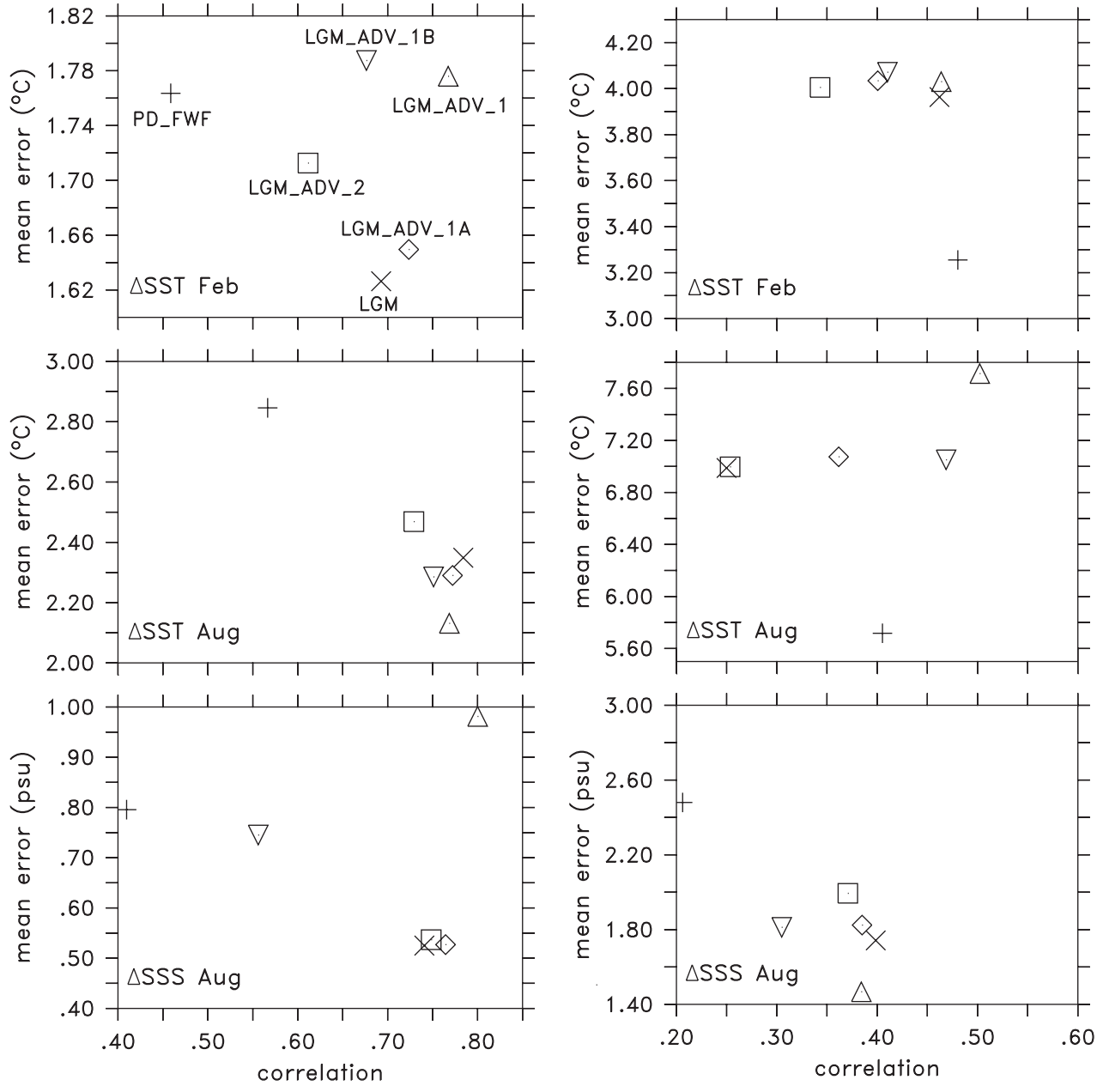

Figure 14. Correlation and basin average error for the different model experiments. Note the different axis labels. (left) SST reconstructions from CLIMAP and SSS data from *Seidov et al.* [1996]. (right) SST and SSS reconstructions from *de Vernal et al.* [2000].

tion of salinity, and therefore the stronger the increase in the north-south salinity gradient. This is also obvious from Figure 13, which suggests that a reduction of the overturning by ~50% is most consistent with the reconstruction (e.g., experiment LGM). In the simulation in which the THC is totally collapsed (LGM_ADV_1), salinities are too low everywhere in the basin, and in the experiment with an increased THC (LGM PD_FWF) the pronounced minimum in the reconstruction is completely absent.

[34] Two measures of the basin-wide model performance with regard to the reconstructions were computed: (1) the correlation coefficient between the model-predicted changes in sea surface properties and the reconstructions and (2) the square root of the basin-averaged (weighted by the grid box area) squared difference between model results and reconstructions. In the following we refer to this second measure as the mean error. The correlation coefficient is insensitive to differences in the basin mean change of SST or SSS as it measures the similarity of the patterns of the changes. The mean error, on the other hand, takes differences of altered basin mean values into account. For these calculations, model results were interpolated to the $2° \times 2°$ grids of the reconstructions.

[35] The plots in Figure 14 show diagrams in which the different model simulations are placed according to these two measures. These diagrams are interpreted by noting that the higher the correlation coefficient and the lower the mean error, the better the agreement between the simulated and the paleoreconstructed fields. That is, the closer a particular experiment is placed to the lower right corner, the better the agreement with the reconstruction. Conversely, the farther up and to the left of the diagram an experiment lies, the worse the agreement with the reconstruction.

[36] In this section we discuss Figure 14 (left), which shows the analysis for the CLIMAP SST and *Seidov et al.* [1996] reconstructions. Figure 14 (right) will be discussed in section 5.4. Unequivocally, the worst simulation is experiment LGM PD_FWF, which was the only run in which the overturning increased. Experiments LGM and LGM_ADV_1A, in which the THC in the Atlantic was reduced by about one half, are in best overall agreement with the reconstructions. Experiment LGM_ADV_1, in which deep water formation was shut off completely, is in slightly better agreement only for the summer SST changes. This is most likely because the model cannot simulate the strong SST minimum around 55°N (see Figure 11), which we discussed in section 5.2. However, the mean error for experiment LGM_ADV_1 is much larger than for experiments LGM and LGM_ADV_1A for winter SST and SSS, thus leading to the conclusion that a collapsed THC is in worse agreement with sea surface property reconstructions compared to a THC, which is reduced by one half. This interpretation depends on assumptions on the accuracy of the reconstructed SST and SSS values. Paleosalinity reconstructions from carbonate oxygen isotopes as used by *Seidov et al.* [1996], for instance, have large error bars, and it is possible that the spatial patterns are more accurately reconstructed than the mean values [*Schmidt*, 1999]. The latter is probably also true for the SST reconstructions. This would imply that the correlation coefficients in Figure 14 are a more reliable measure in the model-data comparison than the mean error and hence that the simulation in which the Atlantic overturning collapsed completely LGM_ADV_1 is best agreement with the reconstructions.

[37] Note that south of 40°N the SSS reconstruction includes very few data points. *Seidov et al.* [1996] used present-day observations to fill the gaps, assuming no large changes between LGM and present day at those latitudes. In order to check if our results are influenced by this procedure we have repeated our analysis with the original data set from *Duplessy et al.* [1991]. We therefore interpolated the modeled SSS anomalies to the locations of 65 sediment cores which were overlapping with the model domain. The results were qualitatively similar to the ones discussed above. None of our conclusions are affected by the treatment of the data gaps and by errors due to the interpolation and extrapolation of the original data into the gridded data set.

[38] From Figure 14 we also see that changes in wind stress, which we regarded negligible for the overturning strength in section 4.2, can significantly affect the distribution of SST and SSS. This can be seen by comparing, e.g., experiments LGM_ADV_1A and LGM_ADV_1B, which lead to quite different results for winter SSTs and SSS despite the very similar THC in both simulations. This also shows the limits of our validation method, which assumes changes in sea surface properties are the result of variations in the THC only.

5.4. GEOTOP Data Set

[39] Here we use a new data set [*de Vernal et al.*, 2000] of sea surface property reconstructions for the glacial North Atlantic from the Research Centre in Isotope Geochemistry and Geochronology (GEOTOP). We use 47 core sites which overlap with our model domain. Anomalies were computed by subtracting present-day observations [*Levitus et al.*, 1994; *Levitus and Boyer*, 1994] from the SST and SSS reconstructions. To facilitate this, we interpolated the present-day observations to the core sites. Modeled anomalies were also interpolated to the 47 core locations in order to compute the mean error and the correlation coefficients.

[40] Figure 14 (right) shows the results for the GEOTOP data set. With regard to the inferred overturning strength for the different simulations, the GEOTOP data lead to ambiguous conclusions. The SST reconstructions, both for winter and summer, clearly favor experiment LGM PD_FWF (increased THC) and are in poorer agreement for runs in which the THC was decreased. The salinity reconstruction, on the other hand, favors experiment LGM_ADV_1, in which NADW formation has completely stopped and shows least agreement with experiment LGM PD_FWF.

[41] The reason for this ambiguity lies in the fact that the GEOTOP SST reconstructions are much warmer than CLIMAP, while the SSS reconstructions are fresher than those from *Seidov et al.* [1996]. All model simulations are significantly colder than the GEOTOP data, so that the warmest experiment (LGM PD_FWF) gives the best agreement. Simulated salinities are higher in all experiments; hence the simulation with the freshest North Atlantic leads to the smallest error. However, even experiment LGM_ADV_1 is too salty compared to the reconstruction. The mean SSS at the 47 sites is 1.28 psu smaller than the present-day observations. For experiment LGM_ADV_1 this reduction is only 0.82 psu. Similarly, the summer SST changes according to the reconstruction are a warming of 0.6°C, while even the warmest simulation (LGM PD_FWF) shows a cooling of 2.5°C. These results suggest that the warm and fresh North Atlantic from the GEOTOP data set cannot be reproduced in any of our simulations. If only the correlation coefficient is considered, the experiment in which the circulation is collapsed (LGM ADV_1) is in best overall agreement with the reconstruction consistent with the result in section 5.3. The large differences between the individual reconstructions clearly require future work in order to solve the discrepancies.

6. Interpretation and Discussion

[42] In section 3 we showed that the reason for the reduced NADW formation in the model simulations of the LGM was the altered freshwater balance of the Atlantic. In Table 2 the total surface freshwater budget of the Atlantic is listed for the different model experiments. The integrated freshwater flux out of the Atlantic is positive (net evaporation) in all experiments. In all fully coupled simulations of the LGM (except LGM PD_FWF) the total net evaporation is reduced compared to the corresponding PD simulation. In other words, the atmospheric export of freshwater out of the Atlantic drainage basin is reduced in the simulations of the Last Glacial Maximum. This is a remarkably robust result considering the fact that two fundamentally different formulations of the atmospheric hydrological cycle were used. We suggest that the reduced moisture content of a colder atmosphere (after the Clausius Clapeyron relation), which leads to a smaller overall water vapor transport, is responsible for the reduced divergence of water vapor from the Atlantic drainage basin. This hypothesis is not only physically plausible but also consistent with the insensitivity of the qualitative model response (reduction of the THC in all cases) to the particular formulation of the atmospheric water vapor transport. However, quantitatively (the amount of the reduction), the response depends on the formulation of the hydrological cycle. Particularly, we have seen that if an advective formulation of the water vapor transport is used, the deep ocean circulation pattern can be altered by dynamical changes of atmospheric low-level winds because of their impact on the Atlantic freshwater balance. Wind changes between the LGM and present day taken from the GFDL atmospheric GCM stabilized the deep water formation in the North Atlantic in our model.

[43] *Ganopolski et al.* [1998] proposed that increased sea ice cover, which inhibits ocean-atmosphere heat flux, is the mechanism responsible for weaker NADW formation during LGM. In order to address this effect in our simulations we examine the modeled sea ice cover in the North Atlantic for experiments PD, LGM, and LGM PD_FWF (Figure 15). The seasonal cycle of sea ice extent in experiment LGM is consistent with recent reconstructions using dinocyst assemblages [*de Vernal et al.*, 2000]. In particular, the south eastern parts of the Nordic Seas are ice free in summer, in agreement with the *de Vernal et al.* [2000] recon-

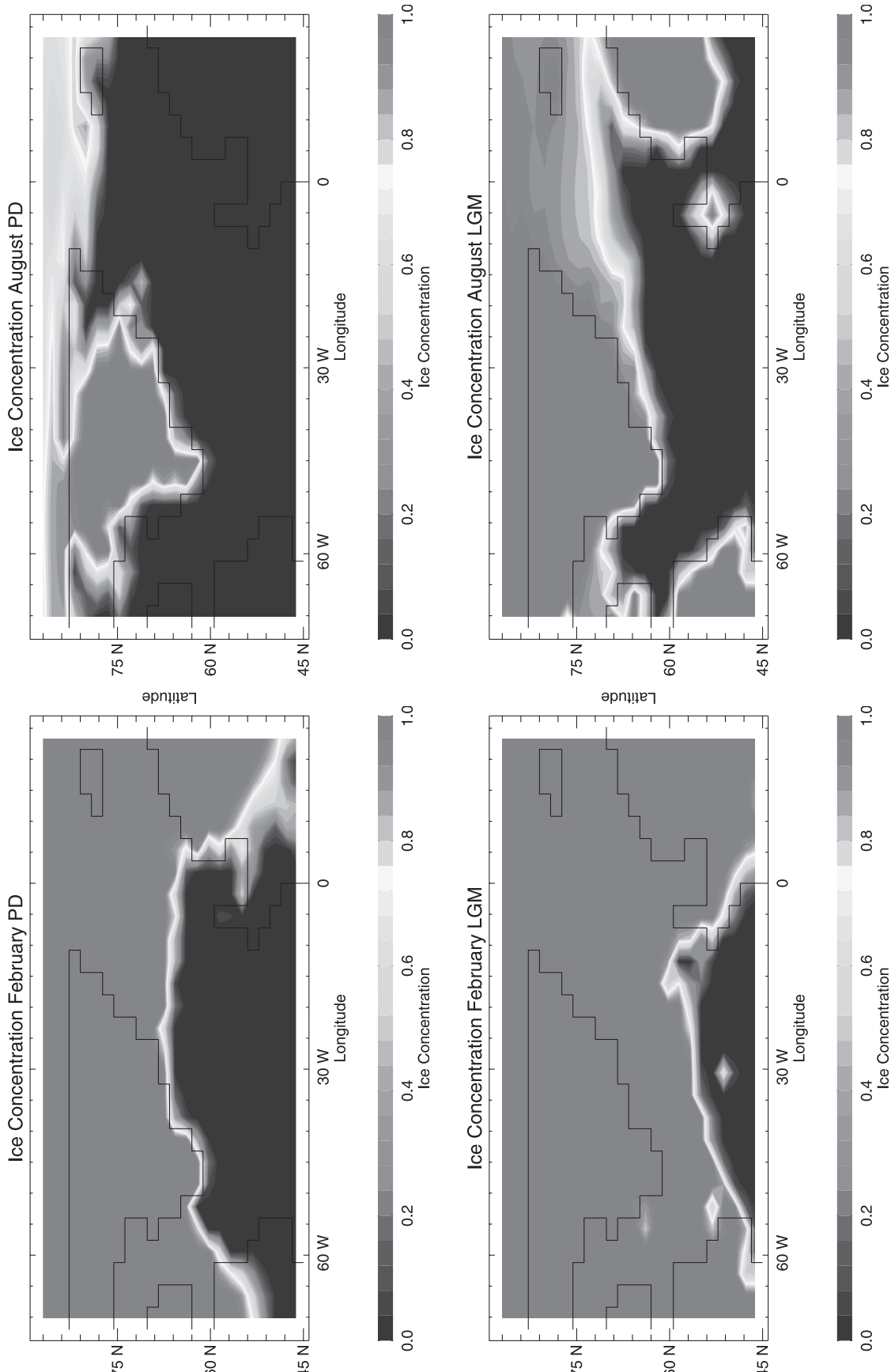

Figure 15. (left) Winter and (right) summer sea ice (over the ocean) and snow (over land) concentrations in the North Atlantic from the present day simulation (PD, top), LGM (middle) and LGM PD_FWF (bottom) experiments. See color version of this figure at back of this issue.

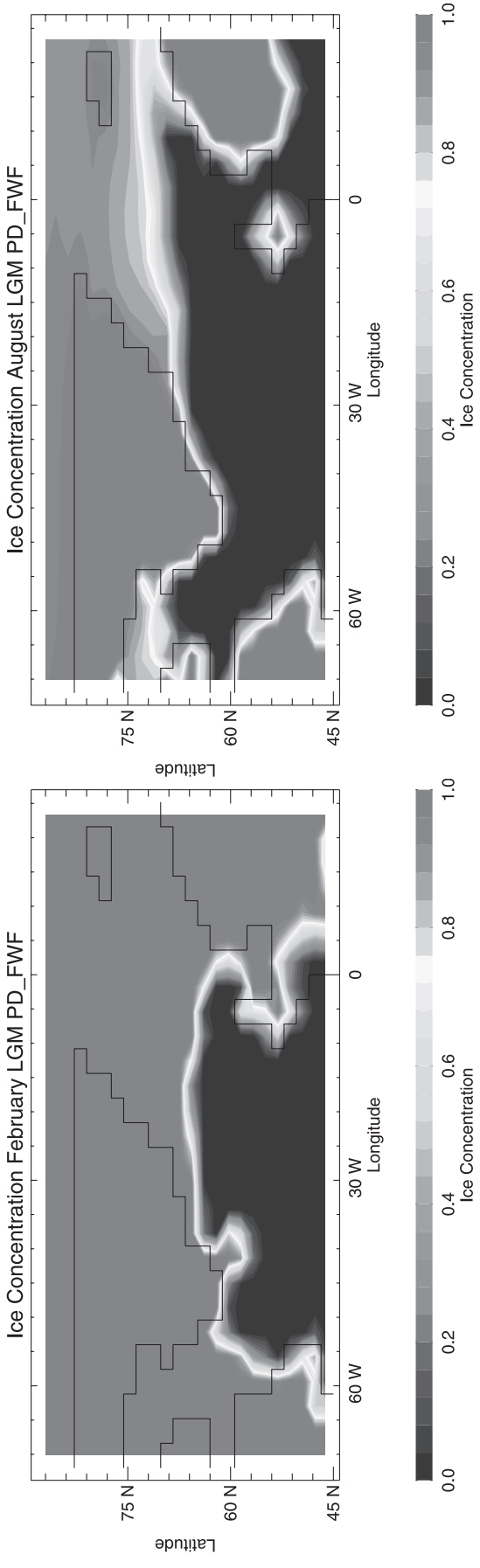

Figure 15. (continued)

struction, whereas CLIMAP data suggest that the Nordic Seas were ice covered even in summer. In the present-day simulation (PD) the southernmost extent of sea ice in winter is ~66°N. In the LGM simulation the sea ice limit is shifted south by ~10°. However, the southward shift of the winter sea ice limit is the consequence of the reduced overturning in experiment LGM. This can be seen from experiment LGM PD_FWF in which the overturning is slightly increased. In this experiment the winter sea ice limit is still around 65°N and not significantly shifted when compared to the PD simulation. Hence the hypothesis discussed above, after which increased sea ice cover is the mechanism responsible for a reduction of the THC during the LGM, cannot be supported by our model results. They rather suggest that the winter sea ice limit is strongly determined by the strength of the overturning and that the reduced THC during the LGM is forced by changes in the atmospheric hydrological cycle.

[44] Some uncertainties concerning this conclusion should be addressed. First, sea ice cover insulates the ocean from heat and freshwater transfer with the atmosphere. In experiment LGM PD_FWF, however, the surface freshwater flux into the ocean is fixed, and hence sea ice cover only diminishes the heat transfer between ocean and atmosphere but has no influence on the freshwater fluxes into the ocean. An examination of the buoyancy fluxes at the deep water formation regions south of the ice edge in experiment LGM PD_FWF shows that the negative buoyancy flux due to freshwater fluxes in regions of net evaporation is very small (not shown). In fact, it is an order of magnitude smaller than the buoyancy flux associated with the heat flux. This suggests that the insulation effect of sea ice in terms of buoyancy transfer is much stronger for the heat flux than for the freshwater flux and, neglecting the latter effect in experiment LGM PD_FWF, does not have a large influence on the deep water formation.

[45] Second, in the present-day simulations, North Atlantic surface waters are systematically too cold in the Nordic seas. This is a problem in most coarse-resolution ocean GCMs, related to the fact that small-scale overflow (over the Greenland-Iceland-Scotland ridge) processes cannot be resolved. This leads to an underestimation of the deep water formation in (and associated heat flux to) the Nordic seas. In reality, the Nordic seas are mostly sea ice free even in winter, while in our model they are mostly ice covered (Figure 15). Thus, we cannot exclude that sea ice-THC feedbacks in the Nordic seas have contributed significantly to the reduced overturning during the LGM, although it seems unlikely that these feedbacks depend on the location of the ice margin. A probably more important uncertainty is also related to unresolved overflow processes. *Lohmann* [1998] suggests that the stability of the North Atlantic THC to meltwater input might be increased if bottom boundary processes are better represented in coarse resolution ocean models. It is not clear if a parameterization of near-bottom flow would also affect equilibrium solutions. However, we believe that this is an important subject for future studies.

[46] As shown in a recent study with the same model including an interactive ice sheet component [*Schmittner et al.*, 2002] multiple equilibria exist in our model for glacial boundary conditions. This study suggests that the equilibria found in our experiments where NADW formation was present are not unique and that another stable steady state with absent NADW formation might also exist for identical boundary conditions. However, the changes in sea surface properties for the equilibrium without NADW are similar to the one from experiment LGM_ADV_1 discussed above.

[47] Reconstructions of SST and SSS provide important constraints on the deep water formation rate and a comparison with model simulations allows one to assess the likelihood of a particular model realization. The comparison of simulated SST and SSS fields with reconstructions from CLIMAP and *Seidov et al.* [1996] lead to the conclusion that modeled sea surface properties are in best agreement with the reconstructions if the Atlantic overturning during LGM is substantially reduced relative to the present day.

[48] No unequivocal conclusion regarding the best agreement between the different model simulations and reconstructions can be drawn for a recent data set [*de Vernal et al.*, 2000] from the northern North Atlantic, which differs considerably from the CLIMAP and *Seidov et al.* [1996] data. Although some effort has been made to explain the differences between the reconstructions [*de Vernal et al.*, 2000], inconsistencies remain. From the viewpoint of large-scale model evaluation, a large spatial coverage of a reconstruction is desirable. We believe therefore that there is an urgent demand for an updated global data set of sea surface property reconstructions for the Last Glacial Maximum, including error estimates. Modelers need to include carbon isotopes C^{13}, C^{14}, and other biogeochemical tracers into their simulations, which would allow more direct comparison with observations and improved estimates of glacial deep water ventilation and circulation.

[49] **Acknowledgments.** Helpful comments by J. Lynch-Stieglitz, D. Seidov, and an anonymous referee and discussions with S.-J. Kim were appreciated. We are also grateful to D. Seidov and J.-C. Duplessy for providing their paleosalinity data sets and to GEOTOP for their reconstructions which we obtained from this web site: http://www.geotop.uqam.ca/geotop/web2/weblgm/IntroductionLGM.shtml. Wind and wind stress data from the GFDL model experiments were kindly provided by A. J. Broccoli. This work was supported by NSERC Operating, Strategic and CSHD research grants. Funding support from the MSC/CICS through the Canadian Climate Research Network is also gratefully acknowledged.

References

Bitz, C. M., M. M. Holland, A. J. Weaver, and M. Eby, Simulating the ice-thickness distribution in a coupled climate model, *J. Geophys. Res.*, *106*, 2441–2464, 2001.

Boyle, E. A., Last-Glacial-Maximum North Atlantic Deep Water: On, off or somewhere in-between?, *Philos. Trans. R. Soc. London, Ser. B*, *348*, 243–253, 1995.

Broccoli, A. J., Tropical cooling at the Last Glacial Maximum: An atmosphere-mixed layer ocean model simulation, *J. Clim.*, *13*, 951–976, 2000.

Bryan, F., High-latitude salinity effects and interhemispheric thermohaline circulations, *Nature*, *323*, 301–304, 1986.

Clark, P. U., A. C. Mix, and E. Bard, Ice sheets and sea level of the Last Glacial Maximum, *Eos Trans. AGU*, *82*, 241–247, 2001.

CLIMAP Project, The surface of the ice-age Earth, *Science*, *191*, 1131–1137, 1976.

CLIMAP Project, Seasonal reconstructions of the Earth's surface at the Last Glacial Maximum, *Geol. Soc. Am. Map Chart Ser.*, *MC-36*, 1981.

de Vernal, A., C. Hillaire-Marcel, J.-L. Turon, and J. Matthiessen, Reconstruction of sea-surface temperature, salinity and sea ice cover in the northern North Atlantic during the Last Glacial Maximum based on dinocyst assemblages, *Can. J. Earth Sci.*, *37*, 725–750, 2000.

Duplessy, J.-C., L. Labeyrie, A. Juillet-Leclerc, F. Maître, J. Duprat, and M. Sarnthein, Surface salinity reconstruction of the North Atlantic Ocean during the Last Glacial Maximum, *Oceanol. Acta*, *14*, 311–324, 1991.

Fanning, A. F., and A. J. Weaver, An atmospheric energy-moisture balance model: Climatology, interpentadal climate change, and coupling to an oceanic general circulation model, *J. Geophys. Res.*, *101*, 15,111–15,128, 1996.

Fichefet, T., S. Hovine, and J.-C. Duplessy, A model study of the Atlantic thermohaline circulation during the Last Glacial Maximum, *Nature*, *372*, 252–255, 1994.

Ganopolski, A., S. Rahmstorf, V. Petoukhov, and

M. Claussen, Simulation of modern and glacial climates with a coupled global model of intermediate complexity, *Nature*, *391*, 351–356, 1998.

Hughes, T. M. C., and A. J. Weaver, Multiple equilibria of an asymmetric two-basin ocean model, *J. Phys. Oceanogr.*, *24*, 619–637, 1994.

Hunke, E. C., and J. K. Dukowicz, An elastic-viscous-plastic model for sea ice dynamics, *J. Phys. Oceanogr.*, *27*, 1849–1867, 1997.

Kalnay, E., et al., The NCEP/NCAR 40 year reanalysis project, *Bull. Am. Meteorol. Soc.*, *77*, 437–471, 1996.

Levitus, S., and T. P. Boyer, *World Ocean Atlas 1994*, vol. 4, *Temperature, NOAA Atlas NESDIS 4*, Natl. Oceanic and Atmos. Admin., Silver Spring, Md., 1994.

Levitus, S., R. Burgett, and T. P. Boyer, *World Ocean Atlas 1994*, vol. 3, *Salinity, NOAA Atlas NESDIS 3*, Natl. Oceanic and Atmos. Admin., Silver Spring, Md., 1994.

Lohmann, G., The influence of a near-bottom transport parameterisation on the sensitivity of the thermohaline circulation, *J. Phys. Oceanogr.*, *28*, 2095–2103, 1998.

Lynch-Stieglitz, J., W. B. Curry, and N. Slowey, Weaker Gulf stream in the Florida Straits during the Last Glacial Maximum, *Nature*, *402*, 644–648, 1999.

Manabe, S., and A. J. Broccoli, The influence of continental ice sheets on the climate of an ice age, *J. Geophys. Res.*, *90*, 2167–2190, 1985.

Manabe, S., and R. J. Stouffer, Two stable equilibria of a coupled ocean-atmosphere model, *J. Clim.*, *1*, 841–866, 1988.

Marchal, O., R. Francois, T. Stocker, and F. Joos, Ocean thermohaline circulation and sedimentary $^{231}Pa/^{230}Th$ ratio, *Paleoceanography*, *15*, 625–641, 2000.

Meissner, K. J., and R. Gerdes, Coupled climate modelling of ocean circulation changes during ice age inception, *Clim. Dyn.*, *18*, 455–473, 2002.

Mikolajewicz, U., and R. Voss, The role of individual air-sea flux components in CO_2-induced changes of the ocean's circulation and climate, *Clim. Dyn.*, *16*, 627–642, 2000.

Mix, A. C., A. Morey, N. G. Pisias, and S. Hostetler, Foraminiferal faunal estimates of paleotemperature: Circumventing the no-analog problem yields cool ice age tropics, *Paleoceanography*, *14*, 350–359, 1999.

Mix, A., E. Bard, and R. R. Schneider, Environmental processes of the Ice Age: Land, Oceans, Glaciers (EPILOG), *Quat. Sci. Rev.*, *20*, 627–657, 2001.

Pacanowski, R., MOM 2 documentation user's guide and reference manual, GFDL Ocean Group technical report, Geophys. Fluid Dyn. Lab., NOAA, Princeton, N. J., 1995.

Peltier, W. R., Ice age paleotopography, *Science*, *265*, 195–201, 1994.

Rahmstorf, S., On the freshwater forcing and transport of the Atlantic thermohaline circulation, *Clim. Dyn.*, *12*, 799–811, 1996.

Rutberg, R. L., S. R. Hemming, and S. L. Goldstein, Reduced North Atlantic Deep Water flux to the glacial Southern Ocean inferred from neodymium isotope ratios, *Nature*, *405*, 935–938, 2000.

Sarnthein, M., et al., Variations in Atlantic surface ocean paleoceanography, 50°–80°N: A time-slice record of the last 30,000 years, *Paleoceanography*, *10*, 1063–1094, 1995.

Schmidt, G. A., Error analysis of paleosalinity calculations, *Paleoceanography*, *14*, 422–429, 1999.

Schmittner, A., M. Yoshimori, and A. J. Weaver, Instability of glacial climate in a model of the ocean-atmosphere-cryosphere system, *Science*, *295*, 1498–1493, 2002.

Seidov, D., and B. J. Haupt, Last glacial and meltwater interbasin water exchanges and sedimentation in the world ocean, *Paleoceanography*, *14*, 760–769, 1999.

Seidov, D., and M. Maslin, North Atlantic Deep Water circulation collapse during the Heinrich events, *Geology*, *27*, 23–26, 1999.

Seidov, D., M. Sarnthein, K. Stattegger, R. Prien, and M. Weinelt, North Atlantic Ocean circulation during the Last Glacial Maximum and subsequent meltwater event: A numerical model, *J. Geophys. Res.*, *101*, 16,305–16,332, 1996.

Semtner, A. J., A model for the thermodynamic growth of sea ice in numerical investigations of climate, *J. Phys. Oceanogr.*, *6*, 379–389, 1976.

Stocker, T. F., D. G. Wright, and W. S. Broecker, The influence of high-latitude surface forcing on the global thermohaline circulation, *Paleoceanography*, *7*, 529–541, 1992.

Tziperman, E., Inherently unstable climate behaviour due to weak thermohaline ocean circulation, *Nature*, *386*, 592–595, 1997.

Weaver, A. J., and E. S. Sarachik, Evidence for decadal variability in an ocean general circulation model: An advective mechanism, *Atmos. Ocean*, *29*, 197–231, 1991.

Weaver, A. J., M. Eby, A. F. Fanning, and E. C. Wiebe, Simulated influence of carbon dioxide, orbital forcing and ice sheets on the climate of the Last Glacial Maximum, *Nature*, *394*, 847–853, 1998.

Weaver, A. J., et al., The UVic Earth System Climate Model: Model description, climatology and applications to past, present and future climates, *Atmos. Ocean*, *39*, 361–428, 2001.

Wiebe, E. C., and A. J. Weaver, On the sensitivity of global warming experiments to the parameterisation of sub-grid scale ocean mixing, *Clim. Dyn.*, *15*, 875–893, 1999.

Yu, E.-F., R. Francois, and M. P. Bacon, Similar rates of modern and last-glacial ocean thermohaline circulation inferred from radiochemical data, *Nature*, *379*, 689–694, 1996.

M. Eby, K. J. Meissner, A. Schmittner, and A. J. Weaver, School of Earth and Ocean Sciences, University of Victoria, P.O. Box 3055, Station CSC, Victoria, British Columbia, Canada V8W 3P6. (katrin@ocean.seos.uvic.ca; andreas@ocean.seos.uvic.ca)

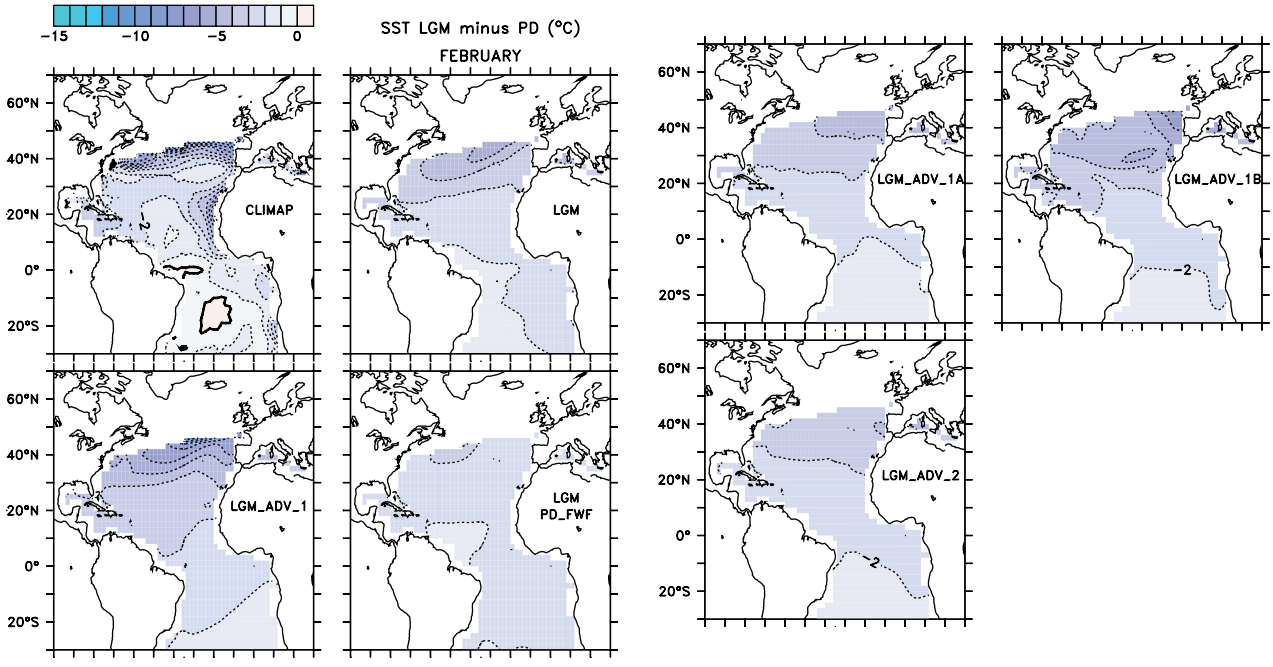

Figure 8. Difference of February sea surface temperatures between the LGM and present day. Top left plot shows CLIMAP reconstruction interpolated to the model grid. Other plots show simulations (experiment name noted over North Africa). Note that only grid points without sea ice in the CLIMAP reconstruction are shown. The model results were masked appropriately.

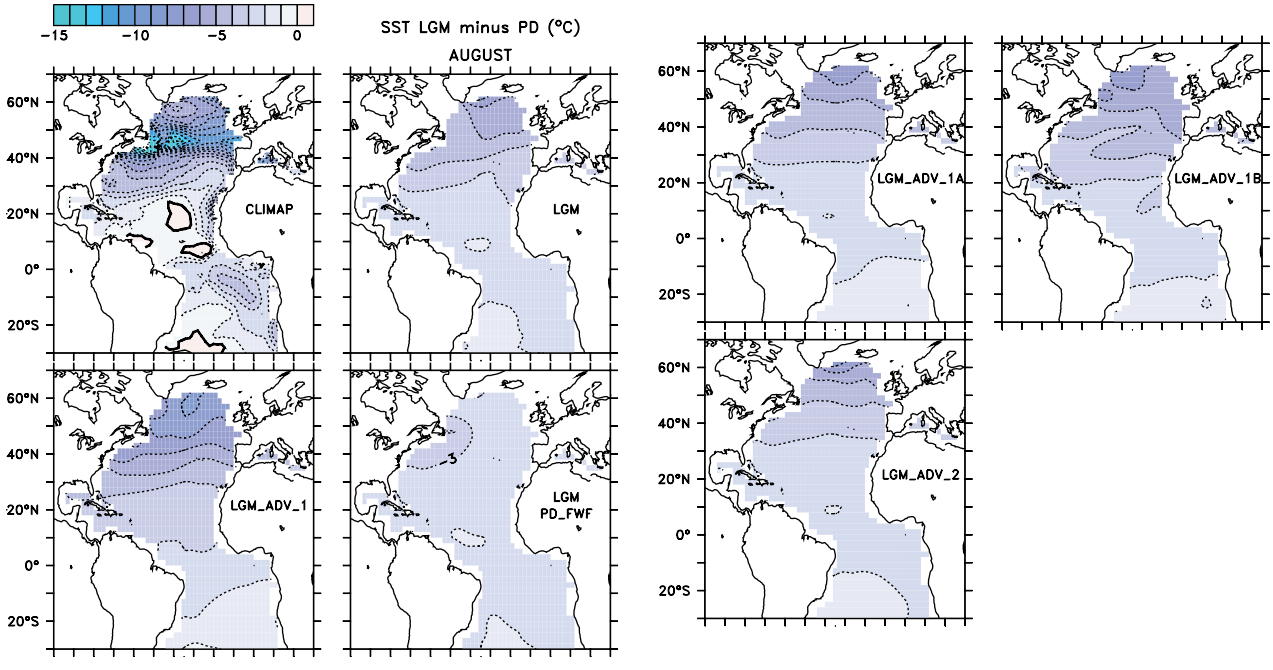

Figure 10. Difference of August sea surface temperatures between the LGM and present day. Top left plot shows CLIMAP reconstruction. Other plots show simulations (experiment name noted over North Africa).

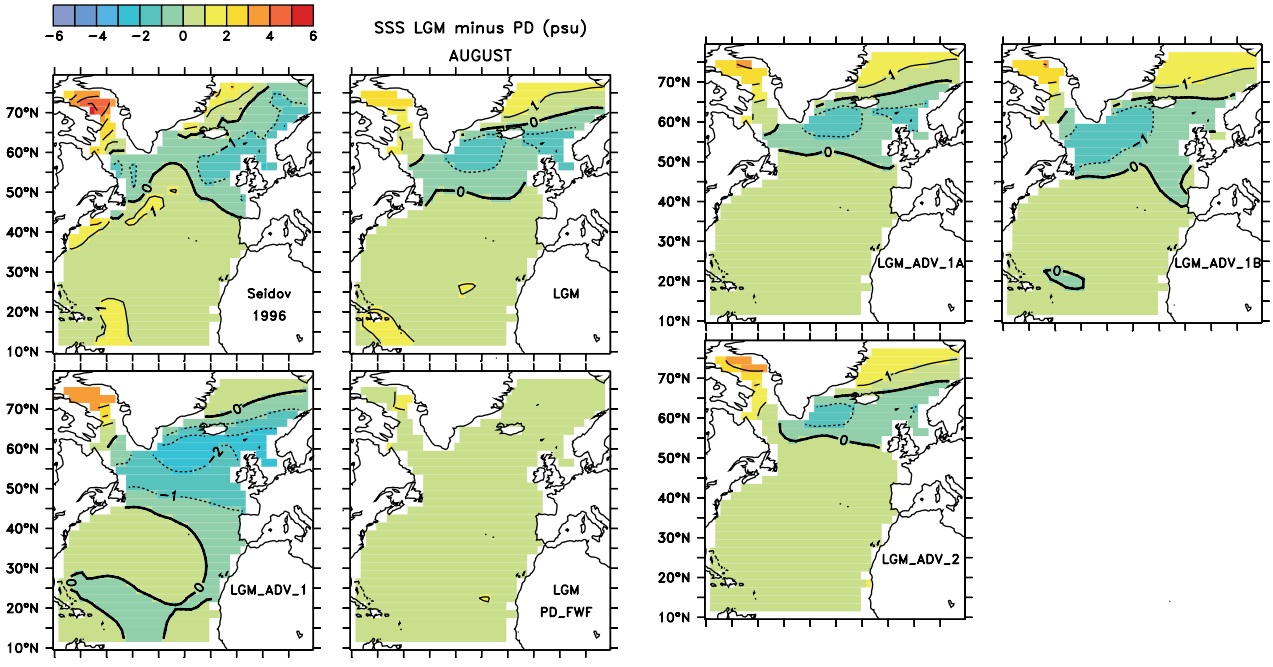

Figure 12. Difference of August sea surface salinities between the LGM and present day. Top left plot shows reconstruction from *Seidov et al.* [1996]; Other panels: simulations (experiment name noted over North Africa).

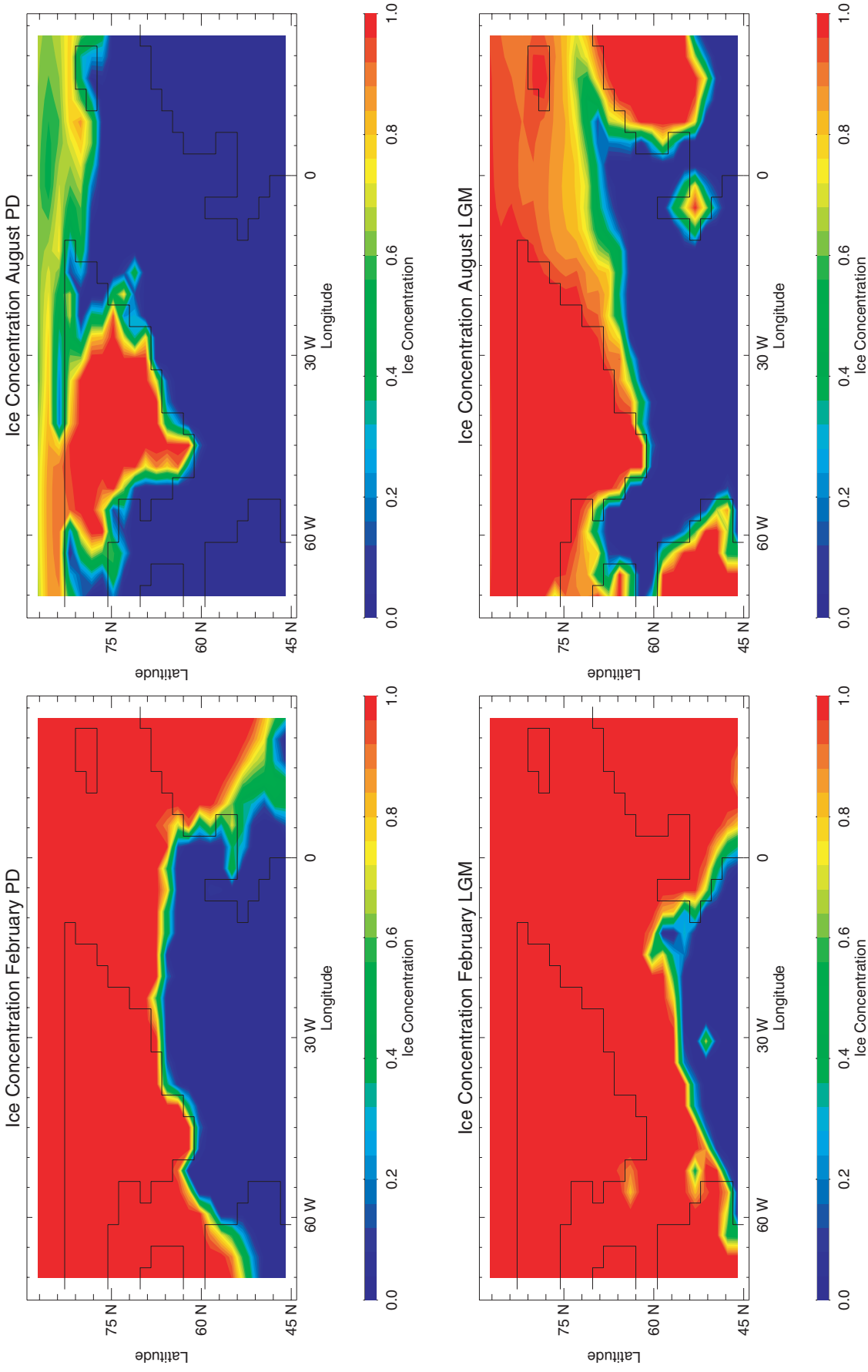

Figure 15. (left) Winter and (right) summer sea ice (over the ocean) and snow (over land) concentrations in the North Atlantic from the present day simulation (PD, top), LGM (middle) and LGM PD_FWF (bottom) experiments.

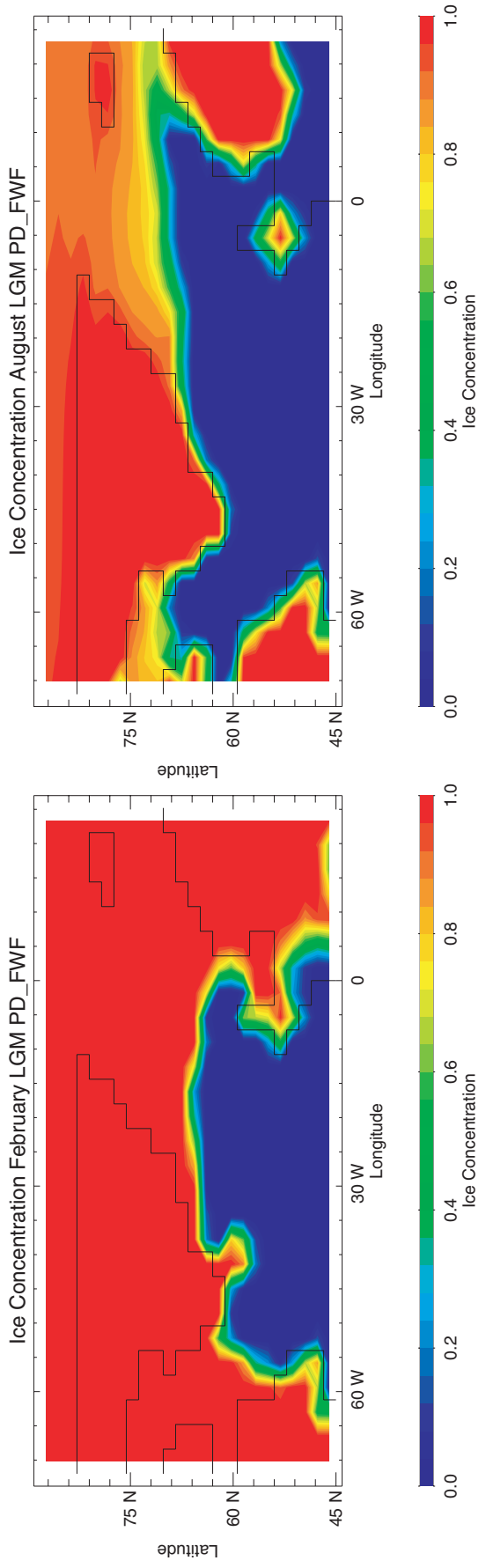

Figure 15. (continued)